Civil Engineering and Environmental Systems
Vol. 26, No. 1, March 2009, 19–33

Taylor & Francis
Taylor & Francis Group

Daily reference evapotranspiration for California using satellite imagery and weather station measurement interpolation

Q.J. Hart[a]*, M. Brugnach[a]†, B. Temesgen[b], C. Rueda[a], S.L. Ustin[a] and K. Frame[b]

[a] *University of California, Davis, Davis, CA, USA;* [b] *California Department of Water Resources, Sacramento, CA, USA*

(*Received 10 October 2007*)

Important water resources in California's agricultural and urban landscapes are at risk without more efficient management strategies. Improved monitoring can increase the efficiency of water use and mitigate these potential risks. The California Irrigation Management Information System (CIMIS) programme helps farmers, turf managers, and other resource managers develop water budgets that improve irrigation scheduling and monitor water stress. The CIMIS system is a repository of meteorological data collected at over 130 computerised weather stations. These are located at key agricultural and municipal sites throughout California and provide comprehensive, timely, weather data collected hourly and daily. In this article, the CIMIS sensor system is combined with hourly NOAA Geostationary Operational Environmental Satellite (GOES) visible satellite data to develop a methodology to extend reference evapotranspiration (ET_0) station estimations to spatial daily ET_0 maps of California. The maps are calculated on a $(2\,km)^2$ grid, a high spatial resolution compared with the density of CIMIS stations. The hourly GOES satellite images are used to estimate cloud cover, which are used in turn to modify clear sky radiation estimates. These are combined with interpolated CIMIS weather station meteorological data to satisfy the Penman–Monteith ET_0 equation.

Keywords: evapotranspiration; satellite imaging; remote sensing; sensor systems

1. Introduction

California experiences periodic water shortages from natural climate variability and is at risk for extended droughts due to changing climate patterns. California agriculture, a $32 billion/year economic sector, requires efficient water management. In California, water conservation is no longer seen as a short-term fix during drought conditions but instead as an on-going practice to be incorporated in the planning process. Water conservation also provides cost savings, improves water quality, contributes to a safe and clean environment, and increases yield. Technologies exist to provide proper water delivery in agricultural, residential, commercial, industrial, and institutional settings. The problem lies in the determination of the right amount of water for various purposes (Temesgen and Frame 2005). Knowledge of these requirements can address a variety

*Corresponding author. Email: qjhart@ucdavis.edu
†Present address. Institute of Environmental Systems Research, University of Osnabrueck, Germany.

ISSN 1028-6608 print/ISSN 1029-0249 online
© 2009 Taylor & Francis
DOI: 10.1080/10286600802003500
http://www.informaworld.com

of water issues such as irrigation scheduling and design, landscape planning, and water transfer. Evapotranspiration is a measurement of the water requirements for the healthy functioning of a particular plant–soil–atmosphere system. The reference evapotranspiration (ET_0) is an evapotranspiration estimate for a standardised grass crop, requiring only meteorological data to calculate. It can then be used to estimate ET of other plants and surfaces.

The California Irrigation Management Information System (CIMIS) programme was introduced by the California Department of Water Resource and the University of California, Davis, in 1982. The primary objective of CIMIS is to provide ET_0 data to California's agricultural growers to influence irrigation scheduling. Although agricultural growers represent the largest user group, the user base has been expanding to include fire fighters, engineers, researchers, educators, landscapers, consultants, meteorologists, lawyers, air quality controllers, and pest managers, among others (Temesgan 2003). CIMIS manages standardised meteorological stations to provide input for the ET_0 calculations. There are over 130 computerised weather stations located at key agricultural and municipal sites throughout California, which provide comprehensive, timely, weather data. The stations continuously collect data 24 hours a day. Local data loggers for each station interrogate the sensors every minute and average 60 consecutive readings for hourly measurements. This hourly data and corresponding daily averages or totals are temporarily stored in the data logger until a centralised facility at the Department of Water Resources (DWR) headquarters retrieves the data for final storage in the CIMIS database. New acquisition software will allow more frequent polling, and CIMIS plans to provide hourly station information. Public access to current and historical data is provided through a web-enabled interface.

CIMIS currently provides ET_0 estimates at specific weather station sites. However, ET is spatially variable, due to a complex interaction between topographical features and the nature of climate itself (Mardikis *et al.* 2005). ET_0 is particularly influenced by solar radiation, which is itself influenced by cloud cover, which cannot be interpolated over large distances from point measurements (Perez *et al.* 1997). Even though point estimates are useful for water managers, these measures still lack the spatial information needed to allow confident decision-making. On average, an arbitrary location in California is about 45 km away from a CIMIS station, a distance potentially beyond the range for CIMIS stations to provide representative measurements. To address the problem of spatial data gaps, other sensor platforms that do excel in monitoring cloud cover and solar radiation are utilised. The National Oceanic and Atmospheric Administration (NOAA) Geostationary Operational Environmental Satellite (GOES) satellites have been used to predict incoming solar radiation using various methodologies for decades (Hay 1993, Noia *et al.* 1993a,b). Noia, for example, divides the techniques into physically and statistically based methods. One of the first and most well-known physical techniques, from Gautier and Diak (1980) and Diak and Gautier (1983), correlates GOES counts to insolation with a three-layer atmospheric model. Using GOES data, cloud cover can be spatially modelled at hourly time or finer increments.

This paper builds on the CIMIS meteorological database by using a methodology that extends the weather station predictions to spatial daily ET_0 maps of California. Because of the spatial variability of the weather variables needed to compute ET_0, as well as the different physical reasons accounting for that variability for each parameter, a direct interpolation of ET_0 was not implemented. Instead, data from the GOES satellite sensor were used to create hourly maps of cloud cover or equivalently, a clear sky factor (K) over California. These K estimations were combined with clear sky solar radiation (R_{so}) predictions modelled with the map grid location and elevation as well as the turbidity of the atmosphere to calculate solar radiation (R_s). Satellite derived K factors were also used in the calculation of net long-wave radiation (R_{nl}), where cloud cover affects the net long-wave radiation exchange between the surface and the atmosphere.

The hourly radiance maps were totalled for the daylight hours and these daily radiance values were combined with weather parameters relating to temperature, wind speed, and humidity,

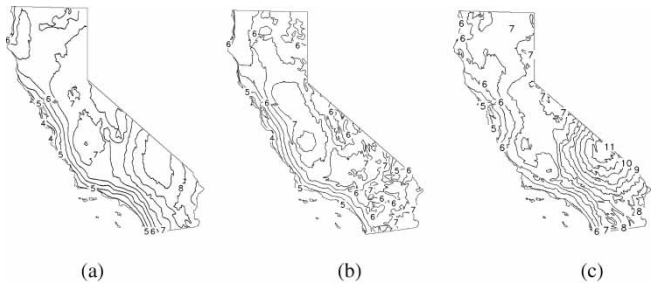

(a) (b) (c)

Figure 1. ET_0 estimations. The scale is in mm/day with isolines on the 0.5 mm/day. (a) Average July ET_0 (b) 2005-07-31 (c) 2007-07-01.

interpolated from the CIMIS weather station sensor data. This combination determines daily ET_0 based on a standard, American Society of Civil Engineers (ASCE), formulation from the Penman–Monteith equation (Allen *et al.* 2005). The maps are calculated on a $(2\,\text{km})^2$ grid, a high spatial resolution compared with the density of CIMIS stations. Implementation details and methodologies used were influenced in part by the need to have a robust operational system in place, allowing for ET_0 estimations in the presence of missing satellite data, or individual weather station malfunctions. The implementation was developed using existing or newly created modules in the Geographic Resources Analysis Support System (GRASS) (Neteler and Mitasova 2004, GRASS Development Team 2006) open-source Geographic Information System (GIS) application. Data have been acquired and ET_0 estimated daily since February 2003. This allows for recent historical data to be used for planning purposes, while daily estimations can inform water managers on variations of these historical averages. As an example of the distribution of ET_0 in California, Figure 1 shows some ET_0 maps of California for July, typically the month with the highest ET_0 values. Figure 1a shows the monthly average ET_0. Daily variations in ET_0, due to changes in the weather parameters, are averaged out, showing relatively smooth regions of constant ET_0. Figures 1b and c show a range of daily variation, where cloud cover or extremes in temperature, humidity, or wind speed can have large and spatially varying effects.

2. ET_0 parameter calculation

Evapotranspiration is the combination of evaporation and transpiration processes. Evaporation is free loss of water from soil and plant surfaces to the atmosphere, whereas transpiration represents the plant mediated transfer of water, mainly through the stomata, to the atmosphere. Evapotranspiration is controlled by physical factors, such as meteorological variables, soil characteristics, and the physiological characteristics of the vegetation such as plant type and biomass. By specifying standard crop parameters with a well-irrigated system, a standard ET_0 can be determined that requires only meteorological measurements. A standardised ET_0 separates atmospheric drivers on ET from crop specifics and reduces the need to develop more complex models for specific crop types and growth stages. Generally, field-specific evapotranspiration parameters are developed as linear relationships to ET_0.

The ASCE Evapotranspiration in Irrigation and Hydrology Committee (ASCE-ET) defines one standardised reference evapotranspiration equation and two reference surfaces (Walter *et al.* 2000, Allen *et al.* 2005). This paper uses the short crop surface as the reference for ET_0, which represents the hypothetical ET from an extensive grass surface of uniform height and actively growing with adequate water. The equation describes the control that environmental factors, such as solar radiation, wind speed, air temperature, and humidity, exert on ET_0. These factors influence

ET either by providing the energy for vaporisation or by increasing efficiency in the removal of water vapour from the surface. The following equations, from the ASCE-ET formulation, describe the parameters in the calculation of ET_0:

$$ET_0 = \frac{0.408\Delta(R_n - G) + \gamma \frac{C_n}{T_m+273} U_2(e_s - e_a)}{\Delta + \gamma(1 + C_d U_2)} \tag{1}$$

$$R_n = R_{ns} - R_{nl} \tag{2}$$

$$R_{ns} = (1 - \alpha) R_s \tag{3}$$

$$R_s = K R_{so} \tag{4}$$

$$R_{nl} = (1.35K - 0.35)(0.34 - 0.14\sqrt{e_a})\sigma \frac{(T_n + 273.15)^4 + (T_x + 273.15)^4}{2} \tag{5}$$

$$e_a = 0.6108 \exp\left(\frac{17.27 T_{dewp}}{T_{dewp} + 237.3}\right) \tag{6}$$

$$e_s = \frac{0.6108}{2}\left(\exp\left(\frac{17.27 T_n}{T_n + 237.3}\right) + \exp\left(\frac{17.27 T_x}{T_x + 237.3}\right)\right) \tag{7}$$

$$\Delta = \frac{4098.17(0.6108)\exp\left(\frac{17.27 T_m}{T_m+237.3}\right)}{(T_m + 237.3)^2} \tag{8}$$

$$\gamma = 0.000665 P \tag{9}$$

$$P = 101.3\left(\frac{293 - 0.0065 z}{293}\right)^{5.26} \tag{10}$$

$$T_m = \frac{T_n + T_x}{2} \tag{11}$$

$$C_n = 900 \text{ and } C_d = 0.34 \tag{12}$$

$R_n - G$ represents the supply of radiative energy available to vaporise water. For daily calculations, net radiation, R_n, is dominant and soil heat flux density, G, is assumed to be negligible. R_n is calculated as the difference between the incoming net short-wave radiation, R_{ns}, and the outgoing net long-wave radiation, R_{nl}, (Equation (2)). R_{ns} represents the portion of R_s that is not reflected, with the reference crop albedo, $\alpha = 0.23$ (Equation (3)). R_s is the amount of incoming solar radiation that reaches the earth surface after accounting for the effects of absorption, scattering, and reflection of the atmosphere. R_s is modelled as a fraction of R_{so}, using a clear sky factor (K). K is directly related to the cloud cover and is determined from GOES satellite data. Various models can be used to calculate R_{so}. The model here uses the clear sky model developed for the European Solar Radiation Atlas (ESRA) and the Heliosat programme (Rigollier *et al.* 2000). In addition to the surface location, the model includes atmospheric attenuation with a turbidity factor, taken from a global atlas. The calculation of ET_0 assumes a standard flat surface when determining R_s. The high relief in California implies that many regions have trends with different slopes and aspects. Some regions utilising these ET_0 estimates may require a correction based on the local slope and aspect. Tian, for example, provides a method to estimate solar radiation for an arbitrary slope and aspect, given solar radiation from a nearby flat terrain (Tian *et al.* 2001). Net long-wave radiation, R_{nl}, represents the exchange of radiation between the crop surface and the atmosphere and clouds (Equation (5)).

Average wind speed at 2 m U_2 is used to calculate the aerodynamic resistance, which represents a resistance to diffusion that air above the vegetative surface imposes on ET. The water content

of the air is represented by $(e_s - e_a)$ expressing the vapour pressure deficit. Saturation vapour pressure, e_s (Equation (7)) describes the daily mean vapour pressure of saturated air. The actual vapour pressure, e_a is calculated as a function of dew point temperature (Equation (6)). The slope of the vapour pressure–temperature curve is Δ (Equation (8)), P represents atmospheric pressure, and γ is the psychrometric constant. T_m represents the mean air temperature (Equation (11)). C_n and C_d are coefficients related to the reference crop used in the equation.

Calculating ET_0 requires meteorological data including air temperature, incoming solar radiation, average daily wind speed and dew point temperature. The CIMIS programme deploys a standardised weather station to measure these parameters. Table 1 lists the sensors deployed at the station. In addition, because ET_0 is defined over a reference surface, the stations themselves are located in a standard environment. This includes maintaining a well-watered irrigated short grass surface surrounding each station.

To develop maps for ET_0, the above parameters need to be calculated for every location in a gridded surface of California. Rather than using station data, solar radiation is derived from models coupled with GOES satellite imagery for a clear sky estimation. Temperatures, wind speed, and dew point are derived by interpolating point data from the network of CIMIS weather stations. Figure 2 shows an overview of all steps for calculating statewide ET_0 maps. In general,

Table 1. CIMIS weather station sensors.

Sensor	Model	Sensitivity
Total solar radiation (pyranometer)	Li-Cor LI200S	±5%
Air temperature	Fenwal UUT5J1 (HMP35)	±0.1°C
Relative humidity	Vaisala Humicap (HMP35)	±2– 4% RH
Wind vane	Met-One 024A	±5%
Anemometer	Met-One 014A	±1.5%
Precipitation	TI TE525M	±1% at 5 cm/h

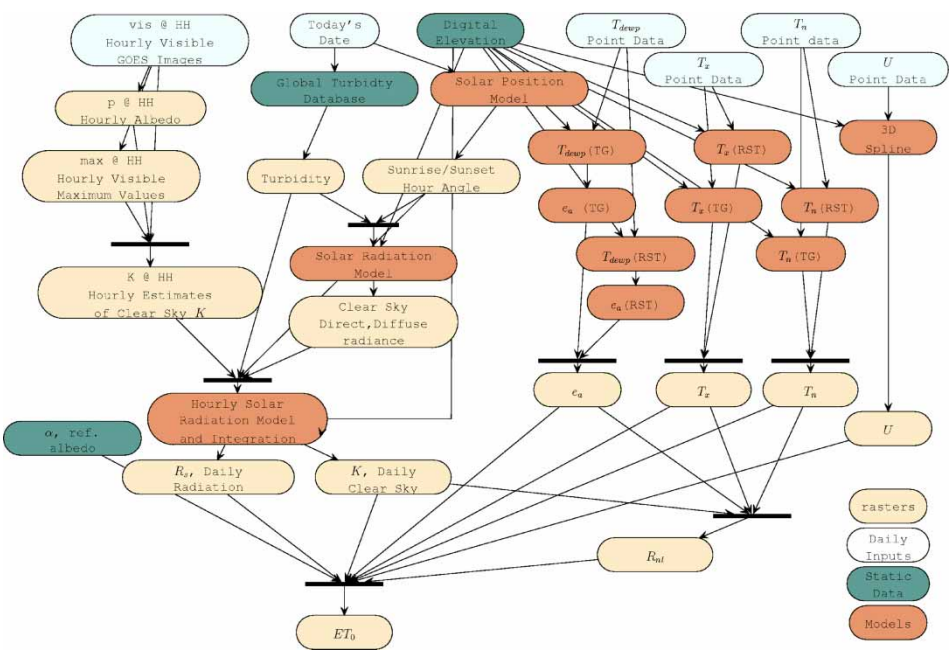

Figure 2. Processing steps for generating ET_0. The left side shows the integration of hourly GOES imagery to estimate radiation parameters. The right side shows weather station interpolations.

the left-hand side describes the process for determining the solar radiance and the right-hand side shows the interpolation of the weather station parameters.

The right-hand side shows four separate parameters that are interpolated from the CIMIS weather station sensors, T_n, T_x, T_{dewp}, and U_2. All interpolation methods take into account elevation differences in the stations as well. Three different methods of interpolation are used. The methods include a 3-D Regularised Spline with Tension for U_2, and two separate methods, Truncated Gaussian (TG) and 2-D Regularised Spline with Tension (RST) with an elevation correction, for temperatures. To determine the amount of clear sky contained at each grid location, GOES visible radiance is compared with both the expected clear sky surface radiance and the expected radiance of a fully developed cloud to determine, K. This is combined with the modelled clear sky radiance. These values are calculated hourly from sunrise until sunset for every day. R_s predictions for each hour are integrated into a daily R_s value. This is compared with the modelled daily R_{so} to determine an average daily K value. The individual maps are combined to determine R_{nl}, R_s, and finally, ET_0. All sensor data processing including the satellite and weather station data are performed using existing or created modules in the GRASS application.

2.1. *Ground station data interpolation*

The daily maximum air temperature at 1.5 m (T_x), daily minimum air temperature at 1.5 m (T_n), dew point temperature at 1.5 m (T_{dewp}), and wind speed at 2 m (U_2) parameters are derived by spatially interpolating point data from the CIMIS network. Spatial interpolation generates surfaces of continuous fields from data collected at discrete locations. A number of different interpolation methods applicable to climatic variables exist, ranging from the most simple (e.g., inverse distance weighting) to more sophisticated ones (e.g., pattern recognition using neural networks). Several authors indicate that simple methods can be used to interpolate climatic variables from a dense and evenly distributed measurement set (Philips and Marks 1996, Antonió *et al.* 2001, Mardikis *et al.* 2005). However, when generating surface climatic data over California using CIMIS data, it is necessary to interpolate over large regions of complex terrain with sparse and unevenly distributed weather stations. The weather stations are spatially distributed as shown in Figure 3. Areas such as California's central valley have a dense distribution of stations, but mountainous, urban, and desert regions are less well represented. This distribution results from the CIMIS

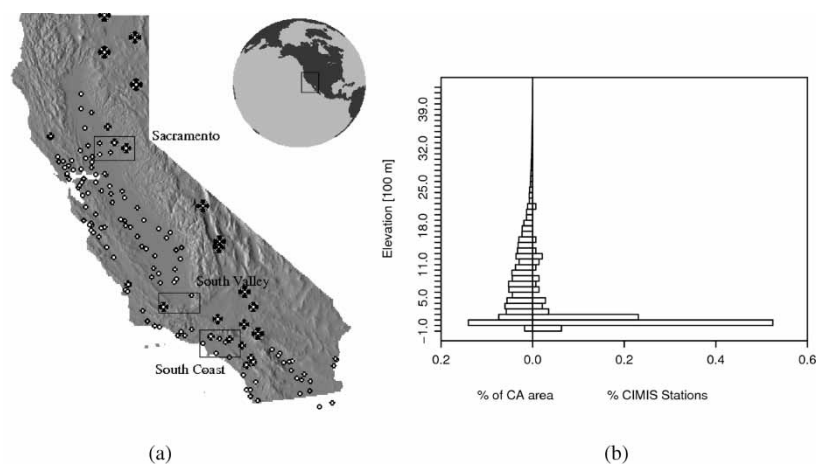

Figure 3. CIMIS weather stations. (a) Station locations, with larger symbols for higher elevations. (b) Histograms of elevations for California versus CIMIS stations.

focus on California's agricultural practices. For various reasons, not all stations report data daily; on average, it is possible to use data from about 120 stations for the interpolations. Figure 3a groups stations by elevation with higher stations having larger symbols. Figure 3a also identifies three regions used to validate temperature changes with elevation. CIMIS stations are also not representative of California in their distribution by elevation. Figure 3b shows the difference in the distribution and range of the elevation, comparing the CIMIS stations and California as a whole. The station elevations under-represent the higher elevations in California.

Several authors have suggested that the incorporation of elevation can improve interpolation results in cases where topography is an important factor to determine climatic variability (Daly *et al.* 1994, Hutchinson 1995, Thornton *et al.* 1997, Price *et al.* 2000). We selected the RST and TG interpolation methods for our parameter estimations, both of which can take into account elevation influences.

The TG method developed by Thornton *et al.* (1997) has been used to generate daily surfaces of temperature, precipitation, and other variables over large regions of complex terrain. The method applies the spatial convolution of a truncated Gaussian filter with a set of observations. The weight $W_{t,\alpha}(r)$ given to an observation with a radial distance r from the centre of the filter, i.e., the estimation point, is given by $W_{t,\alpha}(r) = \exp(-(r/t)^2\alpha) - \exp(-\alpha)$ for $r \leq t$ and 0 for $r > t$. Parameter t determines the truncation distance and parameter α adjusts the shape of the filter. The method is applied as follows. Let $\{(v_i, p_i)\}$ be a set of N observations of a variable V, where v_i and p_i are the observed value and the location of the corresponding station, respectively. The value of the variable $v(p)$ at a point p is estimated by first centring the filter $W_{t(p),\alpha(p)}$ at p, where $t(p)$ and $\alpha(p)$ are the corresponding filter parameters at p. The interpolated value is given by $(v)p = \sum_{i w_i v_i} / \sum_{i w_i}$, where $w_i = W_{t(p)\alpha(p)}(\text{dist}(p, p_i))$.

Terrain elevation is incorporated in the TG method by using a linear regression based correction for the estimated values. The regression is not between values and elevations directly, but on corresponding differences, i.e., between $(v_i - v_j)$ and $(e_i - e_j)$, where (i, j) are all unique pairs of stations over the entire area and e_i is the elevation of station i. Letting a and b denote the obtained regression coefficients, the estimated $v(p)$ is corrected by incrementing $\sum_i [a + b \times (e(p) - e_i)]$ to the basic TG estimation above, where $e(p)$ is the elevation at p.

On a daily basis, the truncation and shape parameters are determined by searching the parameter space and selecting the values that minimise the root mean squared error (RMSE) using a standard leave-one-out cross-validation methodology. In this process, the truncation radius $t(p)$ is initialised to include at least one station from p and then refined via an iterative algorithm such that it is decreased for regions with high observation density and increased otherwise. Although the TG method is applied as an inverse-distance algorithm, the Gaussian function does not force the resultant surface to pass through the observations, thus allowing for smoother surfaces. Figure 4a

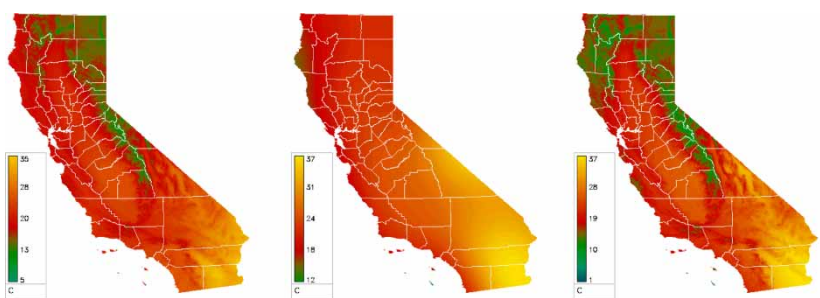

Figure 4. Example of temperature interpolation comparing the RST and TG methods for 1 day, 18 June 2005. (a) The TG method, (b) the 2-D RST on the normalised values, and (c) the final, elevation corrected prediction. Available in colour online.

shows an example temperature calculation for the TG method. (Mitasova *et al.* 1995, Neteler and Mitasova 2004).

RST is a method that simulates passing a flexible plate close to the known data points while minimising the energy to bend the plate. Two parameters determine the outcome of the interpolation. The tension parameter tunes the plate from stiff to flexible. Low tension (stiff) plates are smoother, but can miss high gradient changes. High-tension (flexible) plates are less smooth and allow higher gradient changes about individual points. Tension also controls the influence of neighboring points. Lower tension gives points influence over longer distances. The smoothing parameter controls how much the fitted surface can deviate from the measured point values. Since the spatial interpolation assigns one value for each $(2\,\mathrm{km})^2$ pixel, variation of the RST from the measured points is allowed. Both 2-D and 3-D splines with elevation were used. 2-D RST interpolations along with an elevation normalisation were made for temperature estimations. Wind speed estimations used 3-D splines. Parameter values were selected through cross-validation exercises in conjunction with visual inspection and are constant for all estimates.

The RST interpolation uses a simple elevation dependence to normalise the temperatures from all stations to a standard elevation. The measurements were normalised to sea level using a temperature change rate of 5°C/km. A 2-D spline interpolation was fit to the normalised data. The parameters to the RST were chosen with low tension and high smoothness resulting in a smooth interpolation over the normalised data. The resulting values were then re-corrected with elevation data for California. Figures 4b and 4c shows an example for temperatures calculated using this method.

A rate of 5°C/km was chosen for all temperature interpolations, T_x, T_n, and T_{dewp}. In practice, a consistent elevation dependence of temperature is difficult to show in California. The environmental lapse rate for the normal change in temperature in a vertical profile of air is usually cited as about 6.5°C/km, but this differs from change along a surface with changing elevation. The elevation dependence was determined from yearly averages determined from three areas in the State, labelled in Figure 3a as Sacramento, South Valley, and South Coast. The temperature versus elevation dependence was calculated for all pairs of stations within each region every day over a 3 year period.

As described above, the CIMIS stations do not represent the elevations in California and cannot readily be used to evaluate the two implementations in regions with large elevation differences. The TG method's best fit method can result in large variations in the elevation dependence from day to day, whereas the RST method has a constant dependence on elevation. As neither can be shown to behave definitively better in these high elevation areas, and they depend on somewhat different aspects of the CIMIS station data, the final temperature estimates were generated by averaging the results of TG and RST interpolations.

Despite their differences, both temperature estimations assume a constant elevation dependence throughout the state. An examination of measured temperature change rates between close stations showed rates for California vary widely. While the average change is about 5°C/km for each measurement, the rates show spatial and seasonal variations. Table 2 shows the temperature change rates for the three regions shown in Figure 3 averaged at monthly intervals. Although it is fairly easy to explain the aspects of these results — for example, the diminishing effect of maritime influences in the South Coast region causing an inversion of the rate moving inland with higher elevations — it is clear that simple interpolations over a complex landscape can be only partially successful. Only T_{dewp} shows any statewide stability. These trends are somewhat picked up by the 2-D RST, as shown in Figure 4.

Finally, average daily wind speed measured at 2 m height above the surface is used to compute the aerodynamic resistance, which represents a resistance to diffusion that air above the vegetative surface imposes on ET. Average wind speed maps were generated using 3-D RST. Figure 5 shows some example wind speed interpolations. For these estimates, more flexible surfaces were fit.

Table 2. Average monthly surface temperature change with elevation measurements °C/km for various California regions.

	South Coast			South Valley			Sacramento		
	T_x	T_n	T_{dewp}	T_x	T_n	T_{dewp}	T_x	T_n	T_{dewp}
Jan	−3.34	−3.81	−9.44	3.25	−7.29	−7.66	0.20	−1.93	−4.93
Feb	−3.13	−3.68	−10.22	−3.93	−7.50	−6.48	−4.50	−2.29	−5.62
Mar	0.46	−3.94	−7.58	−4.73	−10.39	−6.14	−5.54	−2.49	−5.49
Apr	−0.46	−3.97	−6.42	−4.67	−10.18	−5.59	−6.50	−2.84	−3.83
May	4.15	−3.09	−6.52	−3.79	−10.69	−5.65	−6.48	−2.43	−3.58
Jun	6.63	−5.31	−3.76	−3.63	−12.83	−5.09	−5.47	−1.27	−3.33
Jul	10.36	−2.38	−4.63	−2.91	−13.02	−6.46	−3.53	2.67	−4.94
Aug	9.99	−2.02	−6.04	−3.23	−12.51	−5.45	−3.09	2.38	−6.50
Sep	6.22	−0.80	−7.30	−3.17	−11.39	−5.39	−4.08	0.81	−6.97
Oct	1.56	−1.68	−5.74	−3.53	−8.34	−6.69	−4.68	−0.33	−5.27
Nov	−2.20	−3.64	−9.45	−0.94	−6.87	−8.38	−2.64	−0.55	−4.56
Dec	−3.05	−3.23	−11.06	1.62	−5.71	−8.43	−2.33	−1.74	−4.28

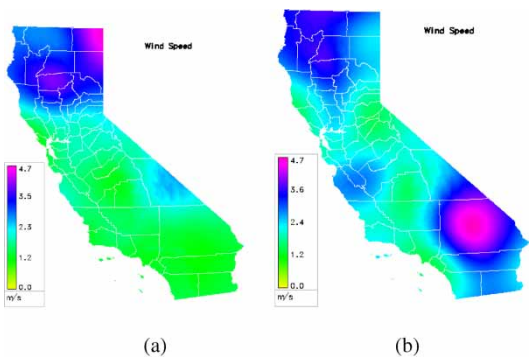

Figure 5. Two typical wind speed interpolations, for a calm 5 and a windy day. (a) 2005/12/21 calm (b) 2005/06/18 windy. Available in colour online.

High winds reported from single stations cause anomalous effects in the interpolation around those points.

2.2. *Radiation models*

Radiative inputs to the ASCE-ET equation include the energy terms; R_s and R_{nl}. Solar radiation can be measured directly for individual point locations or it can be modelled. Upward long-wave radiation is primarily a function of surface temperature and downward radiated long-wave radiation is affected by the cloud cover and water vapour.

2.2.1. *Solar radiation, R_s*

Solar radiation is a linear term in the ET_0 equation and is the driving factor in the ET_0 calculation for much of California. It is important to measure this parameter accurately. CIMIS stations measure solar radiation directly, but this parameter cannot be reliably interpolated spatially over large distances since it is dependent on the cloud cover, which is difficult to interpolate from station data points (Perez *et al.* 1997). GOES satellites, arguably the most important instruments in the meteorological programme of the United States, are part of a programme that has been continuously active for more than 30 years. Its geostationary orbit, essentially remaining motionless

above a point on the equator with respect to the Earth, allows for rapid imager revisits. The high temporal resolution allows GOES to monitor cloud variability and makes it especially well suited for solar radiation modelling.

The method for the calculation of R_s described here combines model predictions of clear sky radiation with hourly estimates of cloud cover using GOES visible channel imager data. This method for estimating solar radiation is independent of measurements at the CIMIS stations. The clear sky solar radiation model used is part of the Heliosat-II programme (Rigollier *et al.* 2000, 2001, Leferve *et al*. 2002). The cloud cover estimates based on the GOES visible channel are based on ratio techniques described by Ellis and Vonder Haar (1976). These methods were chosen as methods that provided small errors and were well suited for daily processing over the relatively small area of California.

For each location in California, the sunrise and sunset times are calculated daily. Within the sunlit period, GOES data are available for each hour, as shown in Figure 6. The solar zenith angle for each hour is shown with solid lines. From each of these hourly GOES images, a clear sky factor is calculated as described in Section 2.2.2. This factor is assumed constant over the intervals of time/sun angle shown with dotted lines. Clear sky radiation is also calculated for each of these intervals. The clear sky radiation and clear sky factor are used to predict the actual radiation for each interval. Finally, the contributions from all intervals are summed for the daily estimate of solar radiation.

The radiation model uses an analytical integration over solar angles and it is simple to change the frequency of the GOES cloud cover estimates. Missing cloud cover estimates, caused by lost GOES images, are handled by extending the intervals adjacent to the missing times. The analytical integration assigns appropriate weights to the remaining cloud cover estimates.

Atmospheric transmission in the model combines aspects of aerosols, relative humidity, ozone, and molecular scattering into a single parameter, the Linke turbidity. This parameter relates the optical depth for an arbitrary atmosphere to an equivalent atmospheric depth of a Rayleigh-only scattering atmosphere. Along with the sun's geometry and the elevation, the predicted radiation is calculated with this parameter. Seasonal values of the Linke turbidity are derived from a world database of turbidity estimates (Remund *et al.* 2003).

2.2.2. *Clear sky factor, K, and solar radiation, R_s*

The GOES imager data are used to calculate hourly estimates of cloud cover. This is a relatively simple method which uses an empirical relation that is roughly a linear relation between a measured

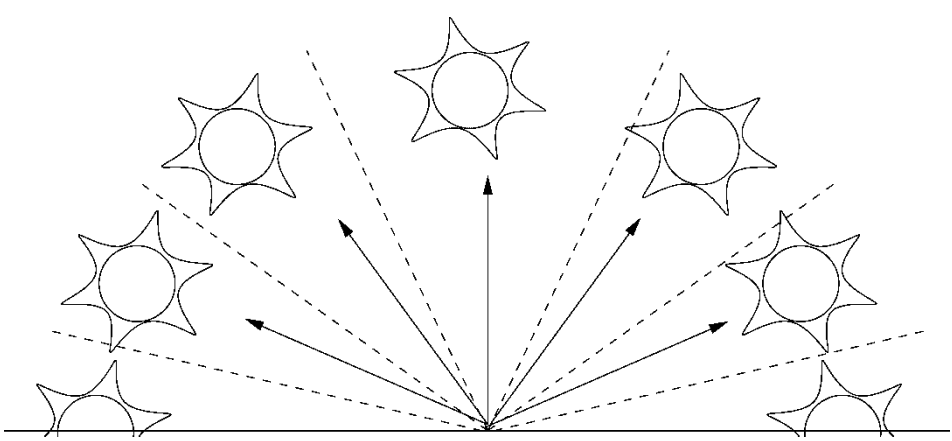

Figure 6. Solar radiation calculations are performed on zenith intervals, using hourly cloud cover estimates.

clearness parameter with K, following a method similar to the Heliosat-II model (Beyer *et al.* 1996, Leferve *et al.* 2002). The clearness parameter, k_i^*, at pixel i is shown in Equation (13).

$$k_i^* = \frac{v_c - v_i}{v_c - v_{g_i}} \tag{13}$$

The clearness parameter is the measure of the amount of cloud cover present at each pixel, i. v_i is the GOES visible radiance, v_{gi} is the expected clear sky radiance from that pixel, and v_c is the maximum expected cloud radiance. k_i^* has a value of one with no clouds, where v_i equals v_{gi} and approaches zero with complete cloud cover as v_i equals v_c. The clear sky radiance, v_{gi}, is calculated for each pixel by taking the minimum measured value of v_i over the previous 2 weeks. This assumes that at some point in that time frame there were no clouds over that pixel. The maximum pixel brightness v_c is calculated by taking the maximum value of *any* pixel for that time in the previous 14 days. To avoid single pixel anomalies, this value is taken on a 9×9 average of the visible image. This results in choosing bright pixels that are part of a large cloudy region. Using these empirical methods for determining v_{gi} and v_c avoids some confounding land surface effects. For example, differences due to changing solar view angles or seasonal changes in the surface are accounted for with the changing albedo values.

The Heliosat-II model (Leferve *et al.* 2002) defined a correction to convert this parameter to a predictive measure of the observed radiance at the surface. The clear sky factor at time i, k_i, as a function of the clearness factor, k_i^*, is shown in Equation (14).

$$k_i = \begin{cases} 1 & 1.0 < k_i^* \\ k_i^* & 0.2 < k_i^* < 1.0 \\ 5k_i^{*2}/3 + k_i^*/3 + 1/15 & -0.1 < k_i^* < 0.2 \\ 0.05 & k_i^* < -0.1 \end{cases} \tag{14}$$

This function is a unity relation for most values of k_i^*, with a correction for low values of k_i^*. The methods for determining v_c imply that for some individual bright pixels, k_i^* can be less than zero. Using these empirical methods for predicting v_{gi} and v_c avoids some confounding land surface effects. For example, differences due to changing solar view angles or seasonal changes in the surface are accounted for with the changing albedo values. With hourly estimates of the clear sky factor,k_i, and the modelled clear sky solar radiation R_{soi}, the daily solar radiation is simply the sum of hourly products, $R_s = \sum_i k_i R_{soi}$. From this, a daily clear sky factor is calculated. This parameter is used to influence energy exchange with the atmosphere in the calculation of emitted long-wave radiation. The clear sky factor (K) is defined as $K = R_s/R_{so}$.

Figure 7 shows a comparison of the predicted and measured daily solar radiation at the CIMIS stations, from February 2003 through April 2006. The best fit correlation is nearly one-to-one when forcing the y-intercept through zero. Allowing the best fit, y-intercept indicates that GOES based estimates may over-predict radiation in low light levels and under-predict radiation in very bright conditions. This could imply that the function mapping cloud brightness to a clear sky factor should be re-evaluated.

The spatial distribution of errors for R_s is not equal over all parts of California as shown in Figure 7b. The error is reported as the root mean squared error between the measurements and predictions. As can be seen, the areas along the coastline and some desert regions have the largest errors. The majority of stations show significantly less difference between measured and predicted R_s. Table 3 shows the variation of the regression parameters computed individually for each month. The table shows little variation in the correspondence between measured and predicted R_s, for the 0 y-intercept case especially. The over-prediction of R_s from the GOES measurements at low light levels generally increases with the available clear sky radiation increases for a particular month.

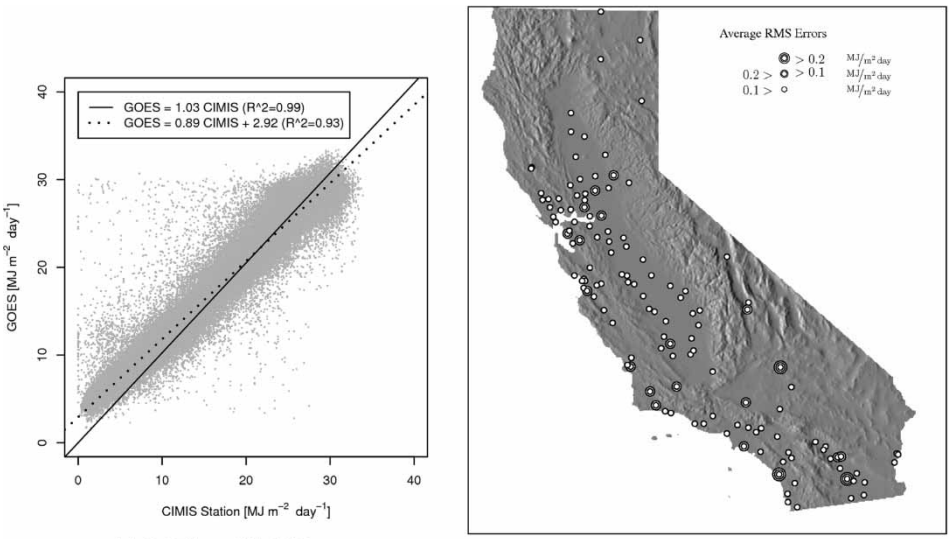

(a) GOES vs. CIMIS R_{ns} (b) Spatial distribution of R_{ns} errors

Figure 7. (a) GOES estimated R_s versus CIMIS measured R_s with two linear fits, one forcing the y-intercept to be 0. (b) Spatial distribution of R_{ns} errors.

Table 3. Monthly variation of GOES versus CIMIS R_s linear fit.

	GOES = mCIMIS + b			GOES = mCIMIS	
	b	m	R^2	m	R^2
Jan	3.9752	0.6805	0.8572	1.083	0.9642
Feb	4.4108	0.7255	0.8202	1.069	0.9732
Mar	4.9344	0.7655	0.8442	1.040	0.9871
Apr	5.297	0.787	0.8361	1.027	0.9876
May	7.1219	0.7468	0.7413	1.022	0.9888
Jun	9.063	0.690	0.6623	1.021	0.989
Jul	12.1926	0.5773	0.5343	1.037	0.9894
Aug	11.5059	0.5708	0.5587	1.049	0.9906
Sep	7.9946	0.6496	0.6317	1.042	0.9887
Oct	5.9819	0.6657	0.7703	1.060	0.9813
Nov	4.8397	0.6366	0.7716	1.083	0.9708
Dec	4.1519	0.6419	0.8271	1.105	0.9556

2.2.3. *Net long-wave radiation,* R_{nl}

The standardised ASCE method for determining net long-wave radiation (R_{nl}) is based on a method developed by Brunt (1932), which uses vapour pressure near the surface to predict net surface emissivity.

$$R_{nl} = (1.35K - 0.35)(0.34 - 0.14\sqrt{e_a})\sigma \frac{(T_x + 273.16)^4 + (T_n + 273.16)^4}{2} \quad (15)$$

Most of these values are based on station measurements with the exception of K. CIMIS estimates cloud cover as a ratio between the measured solar radiation and predicted clear sky radiation; similar to the clear sky factor, K, but with a simpler clear sky radiation model that is a height corrected fraction of the extraterrestrial radiation (Duffie and Beckman 1980, Allen *et al.*2005).

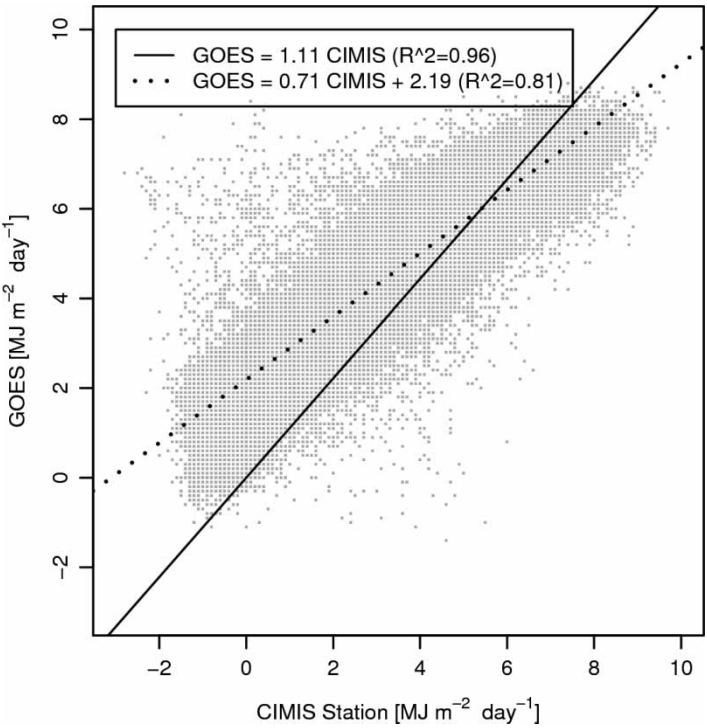

Figure 8. GOES estimated R_{nl} versus CIMIS calculated R_{nl}.

Figure 8 shows the difference between CIMIS R_{nl} and R_{nl} using GOES estimated K factors. As in the R_s comparison, the GOES method over-predicts R_{nl} in the cloudy regions and under-predicts in the clear regions. This may be more pronounced in the R_{nl} comparison because of the difference in the calculation of the cloud factor, K.

2.2.4. *Winter net radiation estimation problems*

Two winter phenomena in California adversely affected the net radiation predictions on certain occasions. These phenomena are snowfall and persistent fog, both common occurrences in California. Both problems cause inaccurate estimations of surface albedo, which lead to inaccurate estimations of cloud cover. These lead in turn to inaccurate estimations of net radiation. In the case of snowfall, the method compares snowfall to the previous albedo and perceives freshly fallen snow as cloud cover, resulting in over predicting clouds and under predicting net radiation. In the case of persistent fog, a 14 day region of continuous fog will cause an over prediction of albedo and will subsequently under estimate cloud cover and over predict net radiation for cloud covered regions. A modification to the existing model could add additional GOES imager channels to help differentiate between cloud and snow, and fog and surface.

3. Conclusions

ET_0 is an important indicator in both agricultural and urban settings and can address water needs for a variety of water issues. We have demonstrated a method of creating daily ET_0 maps for

California by integrating satellite and ground station data, based on the ASCE-ET equation. Maps are created from a combination of hourly GOES data along with interpolations from daily weather station data. The model has been used with GOES and CIMIS data since February 2003, and it will be incorporated in the CIMIS data delivery system, providing users easy access to spatial distributions of ET_0.

Solar radiation is a primary parameter in the ET_0 calculation and comparisons of this technique with historical CIMIS weather station measurements show generally good agreement with measured data. Although comparison of the interpolations can give some indication of the reliability of the interpolations, it is difficult to get an accuracy estimation in areas of the state with limited CIMIS stations. Using other weather stations is difficult because they are not standardised to the height, and surface conditions of the CIMIS stations. Further improvements include obtaining Linke turbidity estimations, used in calculation of R_{so}, from the GOES data directly, or in combination with ground station data. For example, differences in R_s between the CIMIS ground stations and the GOES estimations could be used to determine a point-based turbidity estimation. Separation of the clear sky model and the cloud cover is a convenient simplification. Other methods exist to determine K from the GOES data. For example, the complete Heliosat-II model (Rigollier *et al.* 2001) creates more sophisticated surface models to limit the reliance on hourly ratios. Finally, some events like snowfall and persistent fog lead to erroneous cloud cover predictions. Including additional GOES channels can be included into the methodology to detect these events. We are also comparing the ground station interpolation methods to weather model generated maps of the meteorological parameters to further investigate the spatial distribution of these values.

Nomenclature

Symbol	Description (units)
ET_0	reference evapotranspiration (mm/day)
R_n	net radiation (MJ/m^2 day)
R_{nl}	net long-wave radiation (MJ/m^2 day)
R_s	solar radiation (MJ/m^2 day)
R_{so}	clear sky solar radiation (MJ/m^2 day)
T_n	daily minimum air temperature at 1.5 m (°C)
T_x	daily maximum air temperature at 1.5 m (°C)
T_{dewp}	dew point temperature at 1.5 m (°C)
U_2	wind speed at 2 m (m/s)
T_m	daily mean air temperature at 1.5 m (°C)
e_a	actual vapor pressure (kPa)
e_s	saturation vapor pressure (kPa)
P	atmospheric pressure (kPa)
z	height (m)
γ	psychrometric constant (kPa/°C)
Δ	slope of vapor pressure-temperature curve (kPa/°C)
K	clear sky factor
v_i	GOES visible radiance for pixel i (W/m^2 sr μm)
v_{gi}	GOES clear sky visible radiance for pixel i (W/m^2 sr μm)
v_{ci}	GOES maximum cloud radiance (W/m^2 sr μm)
k_i^*	GOES clearness parameter for pixel i
k_i	GOES clear sky factor for pixel i
σ	Stefan-Boltzmann constant $= 4.903e^{-9}$ (MJ/m^{2}K^4 day)
α	Albedo, 0.23, for the modeled surface

Acknowledgement

This work is supported by the California Department of Water Resources California Irrigation Management Information System (CIMIS) programme, and the NSF Cyberinfrastructure for Environmental Observatories: Prototype Systems to Address Cross-Cutting Needs (CEO:P)I initiative award, Coast-to-Mountain Environmental Transect (COMET).

References

Allen, R.G., *et al.*, eds., 2005. *ASCE standardized reference evapotranspiration equation*. Reston, VA: American Society of Civil Engineers.

Antonió, O., *et al.*, 2001. Spatio-temporal interpolation of climatic variables over large region of complex terrain using neural networks. *Ecological Modeling*, 138, 255–263.

Beyer, H.G., Costanzo, C., and Heinmann, D., 1996. Modifications of the Heliosat procedure for irradiance estimates from satellite images. *Solar Energy*, 56 (3), 207–212.

Brunt, D., 1932. Notes on radiation in the atmosphere. I. *Quarterly Journal of the Royal Meteorological Society*, 58 (2), 389–420.

Daly, C., Neilson, R.P., Phillips, D.L., 1994. A statistical topographic model for mapping climatological precipitation over mountainous terrain. *Journal of Applied Meteorology*, 33, 140–158.

Diak, G.R., and Gautier, C., 1983. Improvements to a simple physical model for estimating insolation from GOES data. *Journal of Climate and Applied Meteorology*, 22, 505–508.

Duffie, J. and Beckman, W., 1980. *Solar Engineering of Thermal Processes*. New York: John Wiley and Sons.

Ellis, J., and Vonder Haar, T., 1976. *Zonal averaged ERB measurements from satellites for climate studies*. Technical Report Atmospheric Science Paper No. 240, Colorado State University, Ft. Collins, CO.

Gautier, C., Diak, G.R., and Masse, S., 1980. A simple physical model to estimate incident solar radiation at the surface from GOES satellite data. *Journal of Applied Meteorology*, 19 (1005–1012).

GRASS Development Team, 2006. *Geographic resources analysis support system (GRASS GIS) software*. ITC-irst, Trento, Italy.

Hay, J.E., 1993. Satellite based estimates of solar irradiance at the earth's surface-I modeling approaches. *Renewable Energy*, 3 (4/5), 381–393.

Hutchinson, M.F., *et al.* 1995. Stochastic space-time weather models from ground based data. *Agriculture and Forest Meteorology*, 73, 237–264.

Leferve, M., Aluisson, M., and Wald, L., 2002. *Description of the software Heliosat-II for the conversion of images acquired be Meteosat satellites in the visible band into maps of solar radiation available at ground level*. Technical report, Ecole Des Mines De Paris, November.

Mardikis, M.G., Kalivas, D.P., and Kollias, V.J., 2005. Comparison of interpolation methods for the prediction of reference evapotranspiration-an application in Greece. *Water Resources Management*, 19, 251–278.

Mitasova, H., *et al.*, 1995. Modeling spatially and temporally distributed phenomena: new methods and tools for GRASS GIS. *International Journal of Geographical Information Systems*, 9 (4), 433–446.

Neteler, M. and Mitasova, H., *Open source GIS: a GRASS GIS approach*. 2nd ed., Boston: Springer.

Noia, M., Ratto, C.F., and Festa, R., 1993a. Solar irradiance estimation from geostationary satellite data: I. statistical models. *Solar Energy*, 51 (6), 449–456.

Noia, M., Ratto, C.F., and Festa, R., 1993. Solar irradiance estimation from geostationary satellite data: II. physical models. *Solar Energy*, 51 (6), 457–465.

Perez, R., Seals, R., and Zelenka, A., 1997. Comparing satellite remote sensing and ground network measurements for the production of site/time specific irradiance data. *Solar Energy*, 60 (2), 89–96.

Philips, D.L. and Marks, D., 1996. Spatial uncertainty analysis: propagation of interpolation errors in spatially distributed models. *Ecological Modeling*, 91, 213–229.

Price, D.T., *et al.*, 2000. A comparison of two statistical methods for spatial interpolation of Canadian monthly mean climate. *Agriculture and Forest Meteorology*, 101, 81–94.

Remund, J., *et al.*, 2003. Worldwide Linke turbidity information. *In*: *Proceedings of ISES solar world congress*, Göteborg, Sweden, June.

Rigollier, C., Bauer, O., and Wald, L., 2003. On the clear sky model of ESRA – European solar radiation atlas – with respect to the Heliosat method. *Solar Energy*, 68 (1), 33–48.

Rigollier, C., Lefèvre, M., and Wald, L., 2001. *The new method Heliosat-II*. Technical Report IST-1999-12245 D3.2, Report to the European Commission, April.

Temesgen, B., CIMIS – past, present, and future. *Water conservation news*, October 2003. California Department of Water Resources.

Temesgen, B. and Frame, K., CIMIS as a tool for water conservation. *Water conservation news*, February 2005. California Department of Water Resources.

Thornton, P.E., Running, S.W., and White, M.A., 1997. Generating surfaces of daily meteorological variables over large regions of complex terrain. *Journal of Hydrology*, 190, 214–251.

Tian, Y.Q., *et al.* 2001. Estimating solar radiation on slopes of arbitrary aspect. *Agricultural and Forest Meteorology*, 109, 67–74.

Walter, I., *et al.* 2000. ASCE's standardized reference evapotranspiration equation. *In*: *American Society of Civil Engineers Watershed Management Conference*, Ft. Collins, CO: American Society of Civil Engineers, p. 11.